Communication

Polarimetric Room Electromagnetics

Troels Pedersen and Ramoni Adeogun

***Abstract*—A polarimetric model for the power delay spectrum for inroom communication is proposed. The proposed model describes the gradual depolarization of the signal with delay. The model is based on the theory of room electromagnetics, specifically the mirror source approach, which is straightforwardly generalized to the polarimetric case. Compared to the previously known unipolarized room electromagnetic models, which are contained as a special case, the new model holds one additional parameter describing the polarization leakage per wall bounce. The proposed model is found to fit well to two sets of polarimetric data one mm-wave and one cm-wave measurements.**

***Index Terms*—Geometrical optics, Indoor propagation, Modeling, Multipath channels, Polarization, Radio propagation.**

I. Introduction

Room electromagnetics [1] has attracted interest from many authors for its ability to characterize the power delay spectrum, i.e., mean power delay profile, of the inroom radio channel. The power delay spectrum is important for the design of communication systems as it determines the mean values of path loss, mean delay, and rms delay spread [2]–[6]. Inspired by methods from room acoustics, models have been derived based on a power balance (or Sabine) approach as in [1], or a mirror source (or Eyring) approach as in [3], [7], [8]. Of the two approaches, it was shown in [3], [9] that the latter approach yields more accurate results for the typical values of wall reflection coefficients encountered in room electromagnetics. The works on room electromagnetics have almost exclusively focused on uni-polarized propagation for simplicity reason. However, polarization is commonly considered important to include in channel models [10] and indeed, numerous recent geometry- and propagation graph-based stochastic channel models such as [11]–[17] account for polarization effects.

An exception to the uni-polarized works in room electromagnetics is the [18] which proposed an polarimetric extension for the distance dependent power delay spectrum model from [2], [3]. This extension was, unfortunately, obtained without actually re-deriving the power delay spectrum from the reverberation theory. The resulting model does not, while being able to fit measurements, link theoretically to the polarimetric propagation mechanisms. Furthermore, the extended model is rather complex in terms of the number of free parameters to be estimated from measurements. This complicates its use as an analytical tool to study how propagation scenario affects the polarized channel.

Inroom measurements, such as [12], [17], [19] suggest that the cross-polar channel, not only show higher power loss, but also exhibit a more gradual onset of the power delay spectrum. Although this behaviour affects important parameters, such as the rms delay spread, a gradual onset is not included in the model [18]. The gradual onset is predicted well by the polarimetric propagation graph model [17] for which the polarimetric power delay spectrum was derived by approximating the graph structure, but not derived from reverberation theory.

Troels Pedersen and Ramoni Adeogun are with Dept. Electronic Systems, Aalborg University, Denmark. {troels,ra}@es.aau.dk. April 28, 2022.

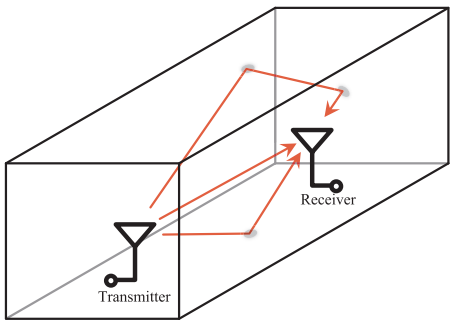

Fig. 1. Rectangular room with transmitter and receiver antennas. Here only three of infinitely many propagation paths are shown.

The present contribution extends the scalar mirror source theory from [3], [4], [8] to the polarimetric case and derive an analytical closed form expression for the power delay spectrum. Compared to scalar room electromagnetics, the derived expression contains, apart from antenna characteristics, only one additional propagation parameter γ specifying the polarization leakage due to wall interactions. The power delay spectrum resembles the one from scalar room electromagnetics, with power decay governed by a reverberation time T. The polarimetric mixing occurs with a different rate described by the polarimetric mixing time T_p given by the room volume, surface area, and cross-polar leakage γ. Furthermore, the cross-polarization ratio (CPR) is also derived for the model. To demonstrate the model we fit it to two sets of measurement data from [12], [17].

II. Considered Scenario

Consider the propagation of radio waves in a box-shaped room with a transmitter and a receiver inside as the one shown in Fig. 1. Waves emitted by the transmitter bounce back and forth between the walls, ceiling, and floor (hereafter referred to as "walls"). The volume of the room is denoted by V and the total wall area is S. The walls are non-ideal conductors and thus in wall interaction (or bounce), a wave is partially reflected back into the room, attenuated, phase-shifted and possibly with altered polarization state. In each bounce a

part of the energy is lost due to absorption in the wall or transmission through it. We assume that the room is isolated in the sense that signals transmitted through walls does not re-enter. Thus we do not distinguish whether signal energy lost due to absorption or transmission.

Directions are specified by the real vector Ω defined as $\Omega = [\cos(\phi)\sin(\theta), \sin(\phi)\sin(\theta), \cos(\theta)]^T$ where θ and ϕ are the coelevation and azimuth (in a right-handed coordinate system with origin at the antenna). The polarimetric power response of an antenna in a specific direction Ω is a two dimensional vector defined as $G(\Omega) = [G_\theta(\Omega), G_\phi(\Omega)]^T$ where $G_{\theta/\phi}(\Omega)$ is the power gain in the θ/ϕ polarization states. The mean polarimetric gain μ is defined as an average over the unit sphere $\mathbb{S}_2$ as

$$\mu = \begin{bmatrix}\mu_\theta \\ \mu_\phi\end{bmatrix} = \frac{1}{4\pi}\int_{\mathbb{S}_2} G(\Omega) d\Omega. \tag{1}$$

For a vertically polarized antenna, $\mu_\phi = 0$. Similarly with $\mu_\theta = 0$ we achieve horizontal polarization. For a lossless antenna, $\mu_\theta + \mu_\phi = 1$ and we may write $\mu = [1-\xi, \xi]^T$ for some constant $0 \le \xi \le 1$. In the following, entities related to the transmitter and receiver are subscripted by t and r, respectively.

Average attenuation and power leakage between polarization states due to a wall bounce is described by a matrix

$$A = g \cdot M, \tag{2}$$

where $0 \le g < 1$ is the average power gain per bounce and the 2×2 matrix M describes the leakage between polarizations.[1] For simplicity, we model M as in [17], i.e.

$$M = \frac{1}{1+\gamma}\begin{bmatrix}1 & \gamma \\ \gamma & 1\end{bmatrix}. \tag{3}$$

The cross-polar leakage per bounce is controlled by the parameter $0 \le \gamma < 1$ which varies with the wall materials. With $\gamma = 0$, no polarization leakage occurs whereas for $\gamma \to 1$, complete depolarization happens after one bounce.

III. Power delay Spectrum Model from Mirror Source Theory

As in [4], [8] we consider mirror source analysis which is easily applied to a box-shaped room. Iteratively mirroring the transmitter in the walls, generates an infinite collection of mirror sources. The signal from each mirror source undergoes successive interactions (bounces) with the wall. In the following, we first derive the power delay spectrum for case where the transmitter is placed uniformly at random within the room. Next, we introduce the necessary modifications for the case where the transmitter-receiver distance is fixed.

[1]The two-polarized case is considered here for simplicity and consistency with previous works on indoor polarimetric models. The model can be extended to the tripolarized case, by replacing M by a 3×3 matrix and using the tri-polarized antenna gain pattern in the following derivations. This leads to only minor change in the resulting model, and is omitted here.

A. Uniformly Distributed Transmitter Position

By assuming the transmitter position to be uniformly distributed within the room, the mirror source positions form a homogeneous point process with intensity equal to $1/V$ [4], [8]. Assuming uncorrelated scattering, the power delay spectrum is of the form

$$P(\tau) = \mathbb{E}\left[\sum_k G_r(\Omega_{r,k})^T \frac{A^{B_k}\lambda^2}{4\pi(c\tau_k)^2} G_t(\Omega_{t,k})\delta(\tau-\tau_k)\right], \tag{4}$$

where the mirror sources are indexed by k and the expectation is taken over the mirror source point process. The speed of light is denoted by c and the wavelength by λ. The signal from mirror source k has direction of departure $\Omega_{t,k}$, direction of arrival $\Omega_{r,k}$ and propagation delay τ_k. The signal is attenuated due to the inverse squared distance power law and a number B_k of bounces. Each bounce attenuates and depolarizes the wave according to the matrix A.

The number of bounces can be approximated as a function of the propagation delay [3]

$$B_k \approx \frac{cS\tau_k}{4V}. \tag{5}$$

As in [4], we assume the mirror source process to be homogeneous and thus the multipath components have uniformly distributed directions of arrival and departure and arrival rate of $4\pi u(\tau)c^3\tau^2/V$, where $u(\tau)$ denotes Heaviside's unit step function. Furthermore with good approximation, the joint intensity function of delays, directions of departure and arrival factorize into a product of intensity function, with one factor for delay, and one for each of the directions.

Invoking Campbell's theorem (see e.g. [20]) and (1) yields

$$P(\tau) = \frac{c\lambda^2}{V}\mu_r^T A^{cS\tau/4V}\mu_t u(\tau), \tag{6}$$

Inserting the eigenvalue decomposition $M = Q\Lambda Q^{-1}$ with

$$\Lambda = \begin{bmatrix}1 & 0 \\ 0 & \frac{1-\gamma}{1+\gamma}\end{bmatrix} \quad \text{and} \quad Q = \frac{1}{\sqrt{2}}\begin{bmatrix}1 & 1 \\ 1 & -1\end{bmatrix}, \tag{7}$$

gives after some manipulations

$$P(\tau) = \frac{c\lambda^2 e^{-\tau/T}}{2V}\Big[(\mu_{r,1}\mu_{t,1} + \mu_{r,2}\mu_{t,2}) \times \left(1 + e^{-\tau/T_p}\right) + (\mu_{r,1}\mu_{t,2} + \mu_{r,2}\mu_{t,1}) \times \left(1 - e^{-\tau/T_p}\right)\Big]u(\tau). \tag{8}$$

Here, T is the usual Eyring reverberation time[2] [3]

$$T = -4V \Big/ cS\ln(g). \tag{9}$$

and T_p is a different time constant which we coin the *polarimetric mixing time*

$$T_p = -4V \Big/ cS\ln\left(\frac{1-\gamma}{1+\gamma}\right). \tag{10}$$

[2]The approximation in (5) can be improved somewhat by using the Kuttruff approach as described in [8]. This will result in a scaling of both T and T_p by a factor depending on the geometry of the room. This modification improves the model's prediction accuracy but is omitted here for simplicity. The modification is straightforward to introduce, if greater accuracy is needed.

The value of γ affects the mixing time dramatically: $\gamma = 0$ gives no polarimetric mixing and $T_p \to \infty$; $\gamma = 1$ gives $T_p = 0$ and the mixing is instantaneous. Naturally, in realistic scenarios, γ lies somewhere in between these two extremes. Fig. 2 plots the model (8) for various parameter settings.

It appears that both reverberation and mixing time are proportional to V/S. Thus, both time constants increase with room size. Comparing rooms with fixed volume, flat and elongated rooms have smaller time constants. We can then define a *mixing constant*

$$\frac{T_p}{T} = \ln(g) \Big/ \ln\left(\frac{1-\gamma}{1+\gamma}\right), \tag{11}$$

which is only dependent on polarimetric leakage and not on room geometry. Fig. 2(a) reports plots of the mixing constant.

The model in (8) contains the classical unipolarized room electromagnetics model [3] as special cases. With $\gamma = 0$, the classical model is recovered; $\gamma \to 1$ gives instantaneous mixing and results in the classical mode scaled by a constant. In between these two extremes, $P(\tau)$ deviates from the usual exponential decay. However, at large delay it approaches the asymptote (included in Fig. 2)

$$\frac{c\lambda^2 e^{-\tau/T}}{2V} \times \left[(\mu_{r,1}\mu_{t,1} + \mu_{r,2}\mu_{t,2}) + (\mu_{r,1}\mu_{t,2} + \mu_{r,2}\mu_{t,1})\right],$$

which equals the classical model up to the bracket term which is unity for lossless antennas.

The power delay spectrum in (8) can be decomposed into a co-polar term

$$P_{\text{co}}(\tau) = \frac{c\lambda^2 e^{-\tau/T}}{2V} (\mu_{r,1}\mu_{t,1} + \mu_{r,2}\mu_{t,2}) \times \left(1 + e^{-\tau/T_p}\right) u(\tau), \tag{12}$$

which has an abrupt onset at $\tau = 0$, and a cross-polar term

$$P_{\text{cross}}(\tau) = \frac{c\lambda^2 e^{-\tau/T}}{2V} (\mu_{r,1}\mu_{t,2} + \mu_{r,2}\mu_{t,1}) \times \left(1 - e^{-\tau/T_p}\right) u(\tau) \tag{13}$$

with a more gradual onset. Their delay-dependent ratio,

$$\frac{P_{\text{co}}(\tau)}{P_{\text{cross}}(\tau)} = \frac{(\mu_{r,1}\mu_{t,1} + \mu_{r,2}\mu_{t,2})}{(\mu_{r,1}\mu_{t,2} + \mu_{r,2}\mu_{t,1})} \times \coth(\tau/2T_p), \tag{14}$$

approaches infinity for small delays and a constant given by the antennas at large delays. The convergence rate of these two terms and thus of the $P(\tau)$ to its asymptote depends on the mixing time.

The CPR can be computed for the model as

$$\text{CPR} = \frac{\int_0^\infty P_{\text{co}}(\tau) d\tau}{\int_0^\infty P_{\text{cross}}(\tau) d\tau}, \tag{15}$$

which after some straightforward manipulations gives

$$\text{CPR} = \frac{(\mu_{r,1}\mu_{t,1} + \mu_{r,2}\mu_{t,2})}{(\mu_{r,1}\mu_{t,2} + \mu_{r,2}\mu_{t,1})} \times \left(1 + 2\frac{T_p}{T}\right). \tag{16}$$

Thus, the CPR is a function of antenna parameters and the mixing constant. Considering the extreme cases:

$$\text{CPR} = \begin{cases} \infty & \gamma = 0 \\ \dfrac{(\mu_{r,1}\mu_{t,1} + \mu_{r,2}\mu_{t,2})}{(\mu_{r,1}\mu_{t,2} + \mu_{r,2}\mu_{t,1})} & \gamma \to 1. \end{cases} \tag{17}$$

For the special case of lossless antennas with perfect cross-polar isolation, the μ vectors have zero/one entries only. If both antennas are vertically polarized, $\mu_t = \mu_r = [1, 0]^T$ we obtain $P(\tau) = P_{\text{co}}(\tau)$, $P_{\text{cross}}(\tau) = 0$, and CPR is infinite; the same results with horizontally polarized antennas, $\mu_t = \mu_r = [1, 0]^T$. Vertical transmit polarization $\mu_t = [1, 0]^T$ and horizontal receive polarization $\mu_r = [0, 1]^T$ gives $P(\tau) = P_{\text{cross}}(\tau)$ and $P_{\text{co}} = 0$ and $\text{CPR} = 0$; the same results with $\mu_t = [0, 1]^T$ and $\mu_r = [1, 0]^T$. We remark that even in the case of unipolarized lossless antennas, the power delay spectrum in (8) deviates from the classical exponential decay.

B. Fixed Transmitter-Receiver Distance

Up until now, the results were derived assuming the transmitter to be placed uniformly at random within the room, irrespective of the distance to the receiver. Now, we modify the expressions for the case where the transmitter is a fixed distance d away from the receiver. This corresponds to conditioning on the mirror source point process, so that a sphere of radius d around the receiver is void of any sources. With reasonably good approximation [4], the conditional intensity of the mirror source process then is $1/V$ everywhere outside this sphere, but zero inside the sphere. The transmitter lie with certainty on the sphere. This gives power delay spectrum conditional on the distance

$$P(\tau|d) = P(\tau)u(\tau > d/c) + P_{\text{dir}}(\tau, d), \tag{18}$$

where $P_{\text{dir}}(\tau, d)$ describes the direct propagation. If the direct path is completely blocked, $P_{\text{dir}}(\tau, d) = 0$. For the line-of-sight case, with fixed antenna orientation, we have

$$P_{\text{dir}}(\tau, d) = G_r(\Omega_{r,\text{dir}})^T G_t(\Omega_{t,\text{dir}}) \frac{\lambda^2}{4\pi d^2} \delta(\tau - d/c). \tag{19}$$

In the latter expression more parameters are needed as we need to specify the value for the scaling constant $G_r(\Omega_{r,\text{dir}})^T G_t(\Omega_{t,\text{dir}})$. If this information is available, it can be included into the model. However, we shall for simplicity assume this constant to equal $\mu_r^T \mu_t = (\mu_{r,1}\mu_{t,1} + \mu_{r,2}\mu_{t,2})$ which corresponds to assuming uniformly distributed orientations. The simplified model reads

$$P_{\text{dir}}(\tau, d) = (\mu_{r,1}\mu_{t,1} + \mu_{r,2}\mu_{t,2}) \frac{\lambda^2}{4\pi d^2} \delta(\tau - d/c). \tag{20}$$

We remark that (18) is the polarimetric extension of the distance-dependent spike-plus-exponential model for the power delay spectrum of inroom channels [2]. Note that the time constants T and T_p remain unchanged, regardless of the transmitter-receiver distance and antenna characteristics.

Plugging the distance dependent power delay spectra into (15) yields

$$\text{CPR}(d) = \frac{(\mu_{r,1}\mu_{t,1} + \mu_{r,2}\mu_{t,2})}{(\mu_{r,1}\mu_{t,2} + \mu_{r,2}\mu_{t,1})} \times \left(Q(d) + \frac{1 + \frac{T_p}{T+T_p} e^{-d/cT_p}}{1 - \frac{T_p}{T+T_p} e^{-d/cT_p}}\right) \tag{21}$$

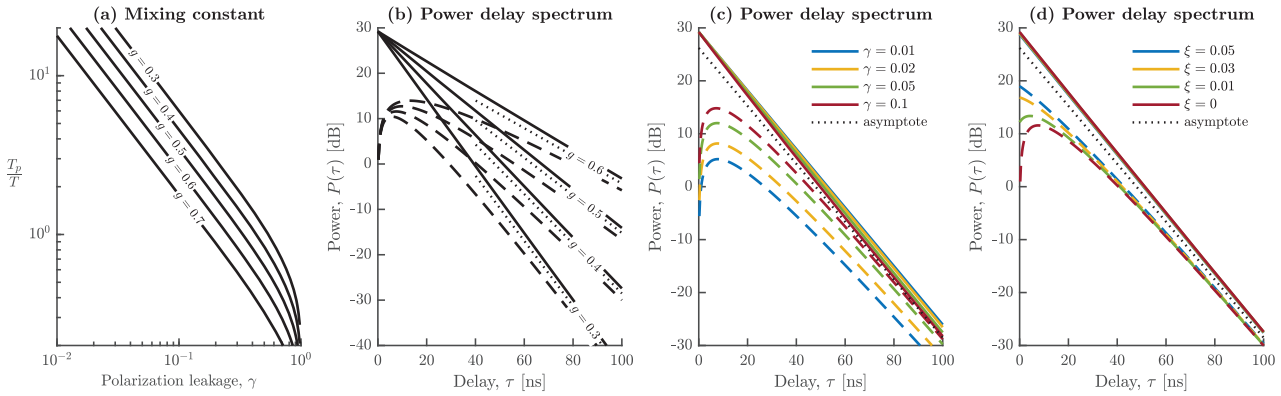

Fig. 2. Theoretical curves for the proposed model; (a) mixing constant with g as parameter; (b)–(d) Power delay spectra room with dimensions $3 \times 4 \times 3\,\mathrm{m}^3$. Solid lines: co-polar case with $\mu_t = \mu_r = [1-\xi, \xi]^T$; dashed lines: cross-polar case with $\mu_t = [1-\xi, \xi]^T$ and $\mu_r = [\xi, 1-\xi]^T$. Asymptotes are given in dotted lines. One parameter is varied in each plot as stated while the remaining parameters are held fixed at values $g = 0.4$, $\gamma = 0.04$, $\xi = 0$. Co-polar curves in (c) and (d) partly overlap as they vary only a little with the parameter.

with the direct propagation term

$$Q(d) = \begin{cases} 0, & \text{in non-line-of-sight} \\ \frac{\frac{\lambda V}{2\pi c T d^2} e^{d/cT}}{1-\left(1+\frac{T}{T_p}\right)e^{-d/cT_p}}, & \text{in line-of-sight.} \end{cases}$$

IV. Application to Measurement Data

We fit the derived model to two sets (M1 and M2) of channel measurements, both obtained with a vector network-analyzer and virtual arrays of vertically and horizontally polarized antennas. The data set M1 from [12] is collected in a furnished meeting room of $3 \times 4 \times 3$ m^3 at center frequency of 60 GHz with a 4 GHz bandwidth. A 5×5 virtual planar array with inter-element spacing of 5 mm was used at both the transmitter and receiver. The resulting 625 realizations were used to obtain the average power delay profile (pdp) for the co- and cross-polar channels. Measurements from both line-of-sight (LOS) and non-line-of-sight (NLOS) measurements are included in the data set. The second data set M2 from [21] is recorded in a $6 \times 10 \times 3$ m^3 furnished conference room at center frequency of 15 GHz with a bandwidth of 1 GHz. Using a virtual 10×10 array at the transmitter and a single monopole at the receiver, gave 100 realizations per polarization. Further details of M1 and M2 are given in [12] and [21], respectively.

The model in Section III characterizes only the propagation effect. The effects of the transmitted signal and measurement noise are included according to

$$P_y(\tau|d) = \int P(\tau - t|d) \cdot |s(t)|^2 dt + P_{\text{noise}}, \qquad (22)$$

where $s(\tau)$ is the transmitted signal and P_{noise} is the power of the additive white measurement noise. Information on the antenna responses are unavailable. Thus we set $\mu_t = \mu_r = [1-\xi, \xi]^T$ and $\mu_t = [1-\xi, \xi]^T; \mu_r = [\xi, 1-\xi]^T$ for the co- and cross-polarized channels respectively.

Parameters g and γ, ξ and P_{noise} are estimated by non-linear least squares fitting (22) (in dB) to the average pdps of the measured co- and cross-polarized channels (also in dB). For M1, the parameters are estimated from one NLOS measurement shown in Fig. 3(a) and used to *predict* the LOS measurements in Fig. 3(b and c). For M2, the fit is shown in Fig. 3(d). The noise power differs between measurements and therefore adapted to each case.

Fig. 3, show clearly that the cross-polar power is present in all four cases. The model fits well both M1 and M2 data as can be seen in Fig. 3(a) and (d). Moreover, the predictions shown in Fig. 3(b) and (c), are also quite accurate. Thus the model allows for making predictions of the LOS case based on data from an NLOS scenario. We remark that model appears to have slightly different slopes of the co- and cross-polarized power delay spectrum at the plotted delay range. However, it can be verified by setting $P_{\text{noise}} = 0$ in (22) that indeed, the two slopes coincide at later delays. The mixing constant has values 11.5 in M1 and 3.7 in M2. Thus gradual polarimetric mixing occurs in both measurements but occurs faster in M2 than M1. We conjecture that this difference is in part due to the difference in frequency and in part caused by clutter from furniture present in the M2.

V. Conclusion

The polarimetric room electromagnetic model was derived based on reverberation theory to describe the power delay spectrum for an inroom channel. We find that depolarization affects the power delay spectrum and thus derived parameters such as rms delay. Depolarization occurs gradually over time due to wall interactions, and is specified in the model by a single leakage parameter. The proposed model is a generalization of the traditional unipolarized room electromagnetic model which is included as a special case. We introduce the polarimetric mixing time to describe the speed at which depolarization occurs. Remarkably, the ratio of mixing time to reverberation time, termed the mixing constant, depend only on material parameters and not on room geometry. We fitted the model to data from a 60 GHz measurement performed

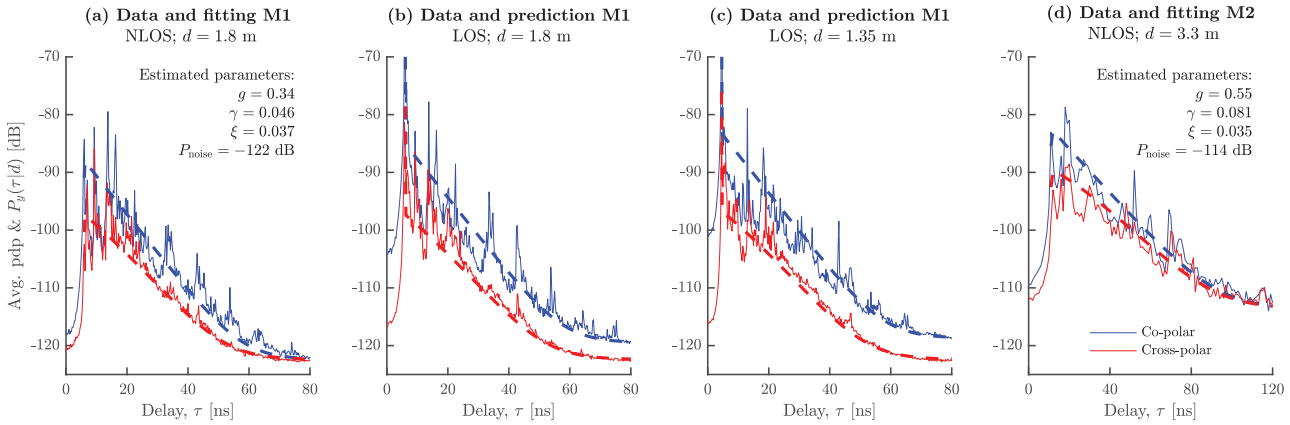

Fig. 3. Comparison of measured average pdp (solid line) to the power delay spectra model (22) (dashed line): (a) Data from office room M1, NLOS, $d = 1.8$ m with fitted model; (b) Data from M1, LOS, $d = 1.8$ m and prediction of model from (a); (c) Data from M1, LOS, $d = 1.35$ m prediction and model prediction of model from (a); (d) Data and model fitting for conference room M2, NLOS, $d = 3.3$ m. The parameter fitting in (a) gives $T = 6.8$ ns, $T_p = 78$ ns and mixing constant of 11.5. For (d) $T = 12.3$ ns, $T_p = 45$ ns and mixing constant of 3.7.

in a small meeting room and a second data set from a 15 GHz measurement obtained in a larger conference room. The model fits well for both data sets, and was successfully used for prediction of unseen data. The mixing constant was found to be eleven and four for 60 GHz and 15 GHz measurements, respectively. These high values indicate that the gradual depolarization is significant for the considered scenarios.

With the proposed model we attempt to capture the average depolarization behaviour using a single free parameter. Thus our derivation relies on a simplistic modelling of depolarization due to wall interactions in a clutter-free environment. Despite the simplistic assumption, we found that the model fits well data from real scenarios where clutter is present. The accuracy can potentially be improved by using a more detailed model at the price of increased complexity, making the model less suited for analytical work.

REFERENCES

[1] J. B. Andersen, J. Ø. Nielsen, G. F. Pedersen, G. Bauch, and J. M. Herdin, "Room electromagnetics," *IEEE Antennas Propag. Mag.*, vol. 49, no. 2, pp. 27–33, Apr. 2007.

[2] G. Steinböck, T. Pedersen, B. H. Fleury, W. Wang, and R. Raulefs, "Distance dependent model for the delay power spectrum of in-room radio channels," *IEEE Trans. Antennas Propag.*, vol. 61, no. 8, pp. 4327–4340, Aug. 2013.

[3] ——, "Experimental validation of the reverberation effect in room electromagnetics," *IEEE Trans. Antennas Propag.*, vol. 63, no. 5, pp. 2041–2053, May 2015.

[4] T. Pedersen, "Stochastic multipath model for the in-room radio channel based on room electromagnetics," *IEEE Trans. Antennas Propag.*, vol. 67, no. 4, pp. 2591–2603, Apr. 2019.

[5] ——, "First- and second order characterization of temporal moments of stochastic multipath channels," in *2020 XXXIIIrd General Assembly and Scientific Symposium of the International Union of Radio Science*, 2020, pp. 1–4.

[6] A. Bharti, R. Adeogun, X. Cai, W. Fan, F.-X. Briol, L. Clavier, and T. Pedersen, "Joint modeling of received power, mean delay, and delay spread for wideband radio channels," *IEEE Trans. on Antennas and Propag.*, pp. 1–1, 2021.

[7] C. Holloway, M. Cotton, and P. McKenna, "A model for predicting the power delay profile characteristics inside a room," *IEEE Trans. Veh. Technol.*, vol. 48, no. 4, pp. 1110–1120, Jul. 1999.

[8] T. Pedersen, "Modelling of path arrival rate for in-room radio channels with directive antennas," *IEEE Trans. Antennas Propag.*, vol. 66, no. 9, pp. 4791–4805, Sep. 2018.

[9] J. She, Y. Yu, P.-F. Cui, W.-J. Lu, and H.-B. Zhu, "Reverberation time and power model in indoor wireless scenarios," *Radioengineering*, vol. 27, no. 2, pp. 485–493, Jun. 2018.

[10] C. Oestges, B. Clerckx, M. Guillaud, and M. Debbah, "Dual-polarized wireless communications: from propagation models to system performance evaluation," *IEEE Trans. Wireless Commun.*, vol. 7, no. 10, pp. 4019–4031, 2008.

[11] F. Quitin, C. Oestges, F. Horlin, and P. D. Doncker, "Polarization measurements and modeling in indoor NLOS environments," *IEEE Trans. Wireless Commun.*, vol. 9, no. 1, pp. 21–25, Jan. 2010.

[12] C. Gustafson, K. Haneda, S. Wyne, and F. Tufvesson, "On mm-wave multipath clustering and channel modeling," *IEEE Trans. Antennas Propag.*, vol. 62, no. 3, pp. 1445–1455, 2014.

[13] X. Yin, Y. He, C. Ling, L. Tian, and X. Cheng, "Empirical stochastic modeling of multipath polarizations in indoor propagation scenarios," *IEEE Trans. Antennas Propag.*, vol. 63, no. 12, pp. 5799–5811, Dec. 2015.

[14] X. Cheng, Y. He, and M. Guizani, "3-d geometrical model for multi-polarized MIMO systems," *IEEE Access*, vol. 5, pp. 11 974–11 984, 2017.

[15] A. Karttunen, J. Jarvelainen, S. L. H. Nguyen, and K. Haneda, "Modeling the multipath cross-polarization ratio for 5–80-GHz radio links," *IEEE Trans. Wireless Commun.*, vol. 18, no. 10, pp. 4768–4778, Oct. 2019.

[16] M. Golmohamadi and J. Frolik, "A geometric scattering model for circularly polarized indoor channels," *IEEE Trans. Antennas Propag.*, vol. 68, no. 3, pp. 2290–2296, Mar. 2020.

[17] R. Adeogun, T. Pedersen, C. Gustafson, and F. Tufvesson, "Polarimetric wireless indoor channel modeling based on propagation graph," *IEEE Trans. Antennas Propag.*, vol. 67, no. 10, pp. 6585–6595, Oct. 2019.

[18] S. Cheng, D. P. Gaillot, E. Tanghe, P. Laly, T. Demol, W. Joseph, L. Martens, and M. Lienard, "Polarimetric distance-dependent models for large hall scenarios," *IEEE Trans. Antennas Propag.*, vol. 64, no. 5, pp. 1907–1917, May 2016.

[19] J. Ø. Nielsen, J. B. Andersen, G. F. Pedersen, and M. Pelosi, "On polarization and frequency dependence of diffuse indoor propagation," in *2011 IEEE Veh. Techn. Conf. (VTC Fall)*. IEEE, Sep. 2011.

[20] M. L. Jakobsen, T. Pedersen, and B. H. Fleury, "Analysis of stochastic radio channels with temporal birth-death dynamics: A marked spatial point process perspective," *IEEE Trans. Antennas Propag.*, vol. 62, no. 7, pp. 3761–3775, Jul. 2014.

[21] Q. Liao, Z. Ying, and C. Gustafson, "Simulations and measurements of 15 and 28 GHz indoor channels with different array configurations," in *Int. Workshop on Antenna Technol.: Small Antennas, Innovative Structures, and Applications (iWAT)*. IEEE, 2017, pp. 256–259.